

Controllable arrangement of integrated obstacles in silicon microchannels etched in 25 wt.% TMAH

Milče M. Smiljanić¹, Branislav Rađenović², Žarko Lazić¹, Marija Radmilović-Rađenović², Milena Rašljčić Rafajilović¹, Katarina Cvetanović-Zobenica¹, Evgenija Milinković¹ and Ana Filipović¹

¹Department of Microelectronic Technologies, Institute of Chemistry, Technology and Metallurgy, National Institute of the Republic of Serbia, University of Belgrade, Njegoševa 12, 11000 Belgrade, Serbia

²Institute of Physics, University of Belgrade, Pregrevica 118, 11080 Belgrade, Serbia

Abstract

In this paper, fabrication of silicon microchannels with integrated obstacles by using 25 wt.% tetramethylammonium hydroxide (TMAH) aqueous solution at the temperature of 80 °C is presented and analysed. We studied basic island patterns, which present union of two symmetrical parallelograms with the sides along predetermined crystallographic directions $\langle 110 \rangle$ ($2\langle 110 \rangle$) and $\langle 100 \rangle$. Acute angles of the parallelograms were smaller than 45°. We have derived analytical relations for determining dimensions of the integrated obstacles. The developed etching technique provides reduction of the distance between the obstacles. Before the experiments, we performed simulations of pattern etching based on the level set method and presented evolution of the etched basic patterns for the predetermined crystallographic directions $\langle 110 \rangle$. Combination of basic patterns with sides along the $\langle 110 \rangle$ and $\langle 100 \rangle$ crystallographic directions is used to fabricate a matrix of two rows of silicon obstacles in a microchannel. We obtained a good agreement between the experimental results and simulations. Our results enable simple and cost-effective fabrication of various complex microfluidic silicon platforms with integrated obstacles.

Keywords: wet etching; level set method simulation; 3D silicon structures; microfluidic platform.

Available on-line at the Journal web address: <http://www.ache.org.rs/HI/>

ORIGINAL SCIENTIFIC PAPER

UDC: 621.9.047-036.8

Hem. Ind. 75 (1) 15-24 (2021)

1. INTRODUCTION

Anisotropic wet etching of a (100) silicon substrate in 25 wt.% tetramethylammonium hydroxide (TMAH) aqueous solution is one of the most common processes in micromachining. Values of etch rates obtained by various authors differ because experiments are performed by various methods [1-4]. Methods used silicon sphere [5-6], maskless etching technique [7-10], trenches in silicon etched by dry reactive ion etching [11] or patterns in the masking layer on silicon wafers (various polygons and circles [12-17]). During the anisotropic wet etching differences in etch rates cause appearance of some crystallographic planes and disappearance of the others. The final three-dimensional (3D) structure is difficult to predict precisely without knowledge of evolution of crystallographic planes during etching. Most of studies considered patterns in the masking layer with the sides along $\langle 110 \rangle$ crystallographic directions. The problem of distortion of convex corners [15,17–20] during etching for these patterns was solved by applying appropriate compensations. The most studied compensations are patterns with the sides along $\langle 100 \rangle$ [9-10,21–25] or along $\langle 110 \rangle$ crystallographic directions [24,26–28]. Fabrication of complex 3D silicon structures was limited as pattern sides were only along the most common directions $\langle 110 \rangle$ and $\langle 100 \rangle$.

In an ideal micromachining design environment, refined control of etched profiles is one of the most important tasks of the manufacturing process. Simulations allow us to reduce the time-consuming and expensive process of refining the

Corresponding author: Milče M. Smiljanić, University of Belgrade-Institute of Chemistry, Technology and Metallurgy, National Institute of the Republic of Serbia ICTM, Department of Microelectronic Technologies, Serbia

E-mail: smilce@nanosys.ihtm.bg.ac.rs

Paper received: 07 August 2020

Paper accepted: 09 February 2021

<https://doi.org/10.2298/HEMIND200807005S>



masks through iterations. Two types of simulations exist: the first category comprises simulators describing the etching process on the atomistic level, usually including the description of etched surface morphologies. However, the most common type of the engineering simulators is the second category, the so-called geometric simulators. This type of simulators deals with the prediction of the etching profile evolution in engineering applications, typically including the combination of etching with other manufacturing techniques. The level set method for evolving interfaces [29] belongs to the geometric type of methods, and it is specially designed for profiles, which can develop sharp corners, change of topology, and undergo orders of magnitude changes in the speed. It is based on a Hamilton–Jacobi type equation for the level set function using techniques developed for solving hyperbolic partial differential equations. Details about the level set simulator used for obtaining results presented here can be found in our previous papers [30,31].

We provided a comprehensive study about etching of patterns with the sides along $\langle n10 \rangle$ crystallographic directions in our previous work [17, 19-20]. Substrates of the (100) silicon were etched in 25 wt.% TMAH aqueous solution at the temperature of 80 °C. We have analysed etching of square patterns with the sides along $\langle n10 \rangle$ crystallographic directions ($0 \leq n < 10$) in [17] and patterns in the shape of parallelograms with sides along predetermined crystallographic directions $\langle n10 \rangle$ ($1 < n < 8$) and $\langle 100 \rangle$ in [19-20]. Parallelograms were designed as islands in the masking layer. In [20], we have obtained sustainable types of 3D silicon shapes during etching. The 3D silicon shapes were the prismoids with parallelograms as the bases [20]. Convex corners of fabricated prismoids were not distorted while we have not applied any convex corner compensation during etching.

This paper is our further work on the (100) silicon etching in 25 wt.% TMAH aqueous solution at the temperature of 80 °C. We analyse the new etching technique for controllable arrangement of silicon prismoids as integrated obstacles in microchannels. In [20] we presented some possible matrices of obstacles obtained from silicon-on-insulator (SOI) wafers, but without any formula necessary for the design of controllable arrangement. In this paper we present novel patterns in the masking layer that reduce distances between obstacles. The diamond-shaped [32-34] and cylinder-shaped [35-37] obstacles are fabricated to disrupt the fluid flow in microchannels and allow better mixing. Also, integrated obstacles are used for particle separation [38-42]. Particle separators utilize the specific arrangement of geometric obstacles within the microchannels to precisely control the particle trajectory and facilitate separation of particles. Most of presented microfluidic platforms are fabricated by using SU-8 resists moulds and polydimethylsiloxane (PDMS) and their application range from mixing a small amount of chemicals [32] to separation [38] of the medical related particles (white blood cells [40], red blood cells [38], circulating tumor cells [41],...). The used obstacles are in various 3D shapes and their matrices influence mixing and trajectory of particles in different ways. Fabricated obstacles in PDMS microchannels were reported to have bases in the shape of circles, parallelograms, and triangles [33-34,38]. In the present paper, we investigated fabrication of rigid silicon obstacles with parallelograms as the bases integrated in a microchannel. Also, we explored the ways to allow a more flexible design that uses wet anisotropic etching. The pattern design in the masking layer and solution anisotropy determines limitations of the obstacle arrangement. Before the etching experiments, we performed level set simulations using two different patterns consisting of parallelograms in the masking layer. These patterns can be used as basic patterns for possible future designs of various silicon based microfluidic platforms for research in the fields of chemistry and personalized medicine.

2. EXPERIMENTAL SETUP

Phosphorus-doped {100} oriented 3" silicon wafers (Wacker, Germany) with mirror-like single polished surfaces and 1-5 Ωcm resistivity have been used in our experiments. SiO_2 was thermally grown at 1100 °C in an oxygen ambient saturated with water vapour. SiO_2 was etched in oxide etch BHF (solution that contains HF, Merck, Germany, ammonia fluoride, Merck, Germany and deionized water) by a standard photolithographic process using laser writer LW405 (MicroTech, Italia) in order to define basic patterns consisting of parallelograms as islands of SiO_2 . After the photolithographic processes, wafers were standardly cleaned. Before etching, the wafers were dipped for 30 s in aqueous solution of HF (10%, Merck, Germany) in order to remove native SiO_2 , and then rinsed with deionized water. Anisotropic etching has been performed in the TMAH 25 wt.% aqueous solution (Merck, Germany) at the temperature of 80 °C. Etching of the whole wafers was carried out in a thermostated glass vessel which was placed on the top of a

hot plate and closed with a Teflon lid, as shown in Figure 1. The TMAH solution temperature was stabilized within ± 0.5 °C by an electronic temperature controller. Evaporation during etching was minimized using the Teflon lid which included a water-cooled condenser. The glass vessel contained roughly 0.8 dm^3 of the solution. The solution was electromagnetically stirred at a velocity of 300 rpm all the time. The wafers were oriented vertically in a Teflon basket inside the glass vessel. The wafers were etched for 52, 85 and 117 min, which correspond to etch depths of 24, 39 and $54 \mu\text{m}$, respectively. The obtained distances were measured by using a laserwriter LW405 (MicroTech, Italia) and an interference microscope Epival Interphako (Carl Zeiss, Germany).

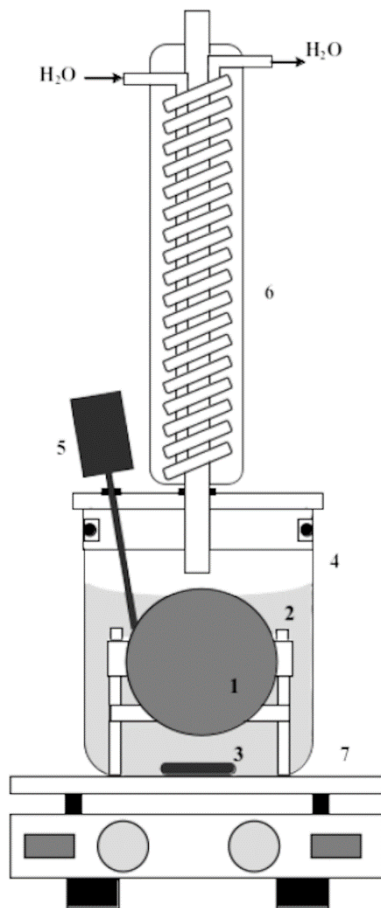


Figure 1. Schematic diagram of the experimental setup [43]: 1 - silicon wafer; 2 - Teflon basket; 3 - magnetic stir bar; 4 - thermostated glass vessel closed with a Teflon lid; 5 - electronic temperature controller; 6 - water-cooled condenser; 7 - hot plate.

3. RESULTS AND DISCUSSION

In our previous work [20], we have presented and analysed parallelograms with sides along predetermined crystallographic directions $\langle n10 \rangle$ ($1 < n < 8$) and $\langle 100 \rangle$. Acute angles of parallelograms α_{n10} were smaller than 45° . During the etching, we have obtained sustainable silicon prismoids with parallelograms as the bases. The sidewalls of prismoids were defined only by the $\{n11\}$ and $\{100\}$ families. Table 1 provides undercut ratios U_{n11} of crystallographic planes that appear during etching of islands in the masking layer [20]. Together with the total etch depth d_{100} , the undercut ratio defines the sizes of the mask in the shape of parallelogram. Because of these two parameters, the minimal distance between two fabricated silicon prismoids is limited and only certain arrangements of obstacles are possible in the microchannels. Distance between vertices M and Q of the etched obstacles, as shown in Figure 2a, is given by the following equations:

$$U_{n11} = \frac{r_{n11}}{r_{100} \sin \gamma_{n11}} \quad (1)$$

$$d_{n10} = U_{n11} d_{100} \tag{2}$$

$$X_{P \rightarrow Q} = X_{N \rightarrow M} = \frac{d_{n10}}{\sin \alpha_{n10}} + \frac{d_{100}}{\text{tg} \alpha_{n10}} \tag{3}$$

$$Y_{P \rightarrow Q} = Y_{N \rightarrow M} = d_{100} \tag{4}$$

$$d_{MQ} = 2 \left(\frac{d_{n10}}{\sin \alpha_{n10}} + \frac{d_{100}}{\text{tg} \alpha_{n10}} \right) + d_{NP} = 2d_{100} \left(\frac{U_{n11}}{\sin \alpha_{n10}} + \frac{1}{\text{tg} \alpha_{n10}} \right) + d_{NP} \tag{5}$$

where $X_{P \rightarrow Q}$, $Y_{P \rightarrow Q}$ and $X_{N \rightarrow M}$, $Y_{N \rightarrow M}$ are absolute displacements of vertices in x and y directions ($\langle 100 \rangle$ crystallographic directions), d_{NP} is the initial distance between vertices N and P of the mask pattern, d_{MQ} is the distance between vertices M and Q at the end of etching, d_{n10} is the undercut distance along one $\langle n10 \rangle$ side of the parallelogram, r_{n11} and r_{100} are the etch rates of $\{n11\}$ and $\{100\}$ crystallographic planes, respectively, γ_{n11} is the angle between $\{n11\}$ and $\{100\}$ crystallographic planes, and α_{n10} is the angle between $\langle n10 \rangle$ and $\langle 100 \rangle$ crystallographic directions. Values of r_{n11} and γ_{n11} are given in Table 1 [17], values of α_{n10} in Table 2, while r_{100} equals to $0.46 \mu\text{m}/\text{min}$. Parallelograms change their heights in the masking layer during etching according to:

$$h_{100\text{etched}} = h_{100} - 2d_{100} \tag{6}$$

$$h_{n10\text{etched}} = h_{n10} - 2 \frac{r_{n11}}{r_{100} \sin \gamma_{n11}} d_{100} = h_{n10} - 2U_{n11} d_{100} = h_{n10} - 2d_{n10} \tag{7}$$

where h_{100} and $h_{100\text{etched}}$ are the heights of the parallelogram side along $\langle 100 \rangle$ crystallographic direction before and after etching, respectively, while h_{n10} and $h_{n10\text{etched}}$ are the heights of the parallelogram side along $\langle n10 \rangle$ crystallographic direction before and after etching, respectively. Parameters $2d_{100}$ and $2U_{n11}d_{100}$ define the sizes of the smallest structures that would not be undercut during etching [20].

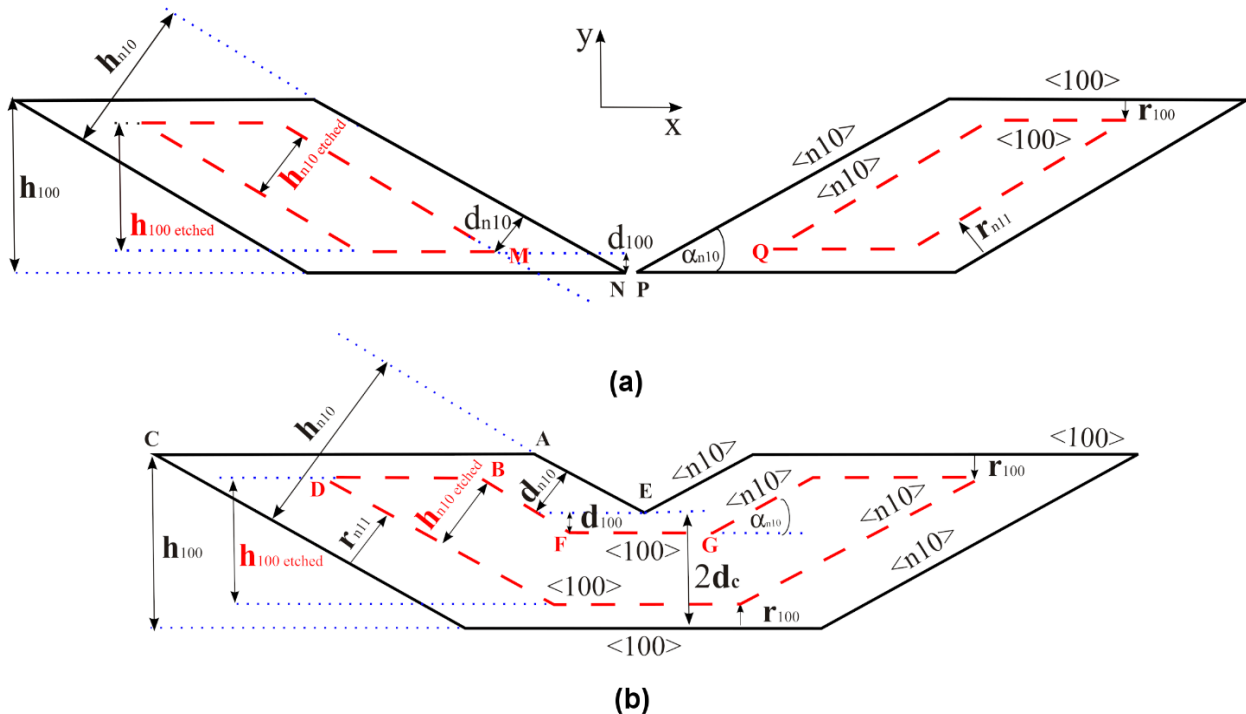


Figure 2. Schematic representation of evolution of the etching pattern. a) Etching of separate island patterns in the shape of parallelogram. b) Etching of the first basic pattern that presents union of two symmetrical parallelograms.

Here, we present the etching technique to reduce the distance between fabricated prismoids. We analysed two different patterns consisting of parallelograms in the masking layer, as shown in Figures 3-5. Patterns are islands of

silicon dioxide. The first pattern presents union of two symmetrical parallelograms with the sides along predetermined crystallographic directions $\langle n10 \rangle$ ($2 < n < 8$) and $\langle 100 \rangle$, as shown in Figures 2b, 3, and 4. The second pattern is designed as an extended version of the first one, and it presents a basic pattern for a matrix of obstacles, as shown in Figure 5. The main idea behind the designed patterns is based on the results of our previous work [17], where we explored etching of square apertures with the sides along $\langle n10 \rangle$ crystallographic directions. In cases $n > 1$, the initial right concave corners turned into three new concave corners during etching. One of the angles is formed by $\langle n10 \rangle$ and $\langle 100 \rangle$ crystallographic directions (angles F, G in Figure 2b) and the value of the concave angle in the masking layer is $180 + \alpha_{n10}$, Table 2. Sidewalls of the concave angle are also defined by planes of the $\{n11\}$ and $\{100\}$ families as in the case of the etched island in [20]. The initial angle E, formed by two symmetrical $\langle n10 \rangle$ crystallographic directions, as shown in Figure 2b, turned into two new concave corners (angles G, F) during etching, as shown in Figures 3-5. Sidewalls of new concave corners are defined by two planes from $\{n11\}$ family and one shared plane of $\{100\}$ family.

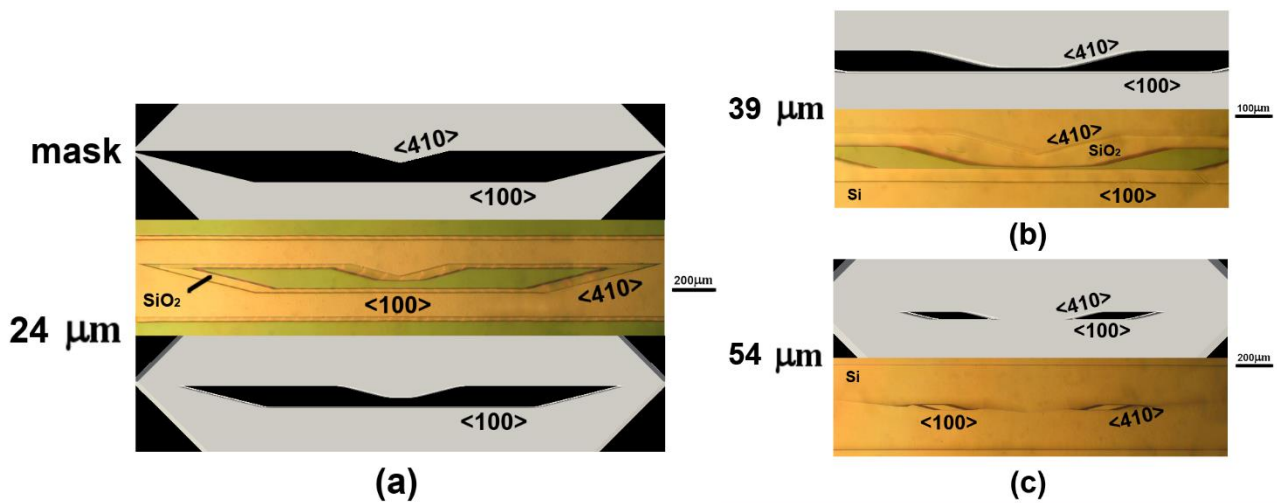


Figure 3. Simulated etching profiles and microphotographs of the first basic pattern with the sides along $\langle 100 \rangle$ and $\langle 410 \rangle$ crystallographic directions: a) Initial mask in the SiO_2 masking layer and 3D silicon structure after etching of $24 \mu\text{m}$. b) The etch depth is $39 \mu\text{m}$. c) The etch depth is $54 \mu\text{m}$. SiO_2 is removed after reaching the etch depth of $54 \mu\text{m}$

Table 1. Angles γ_{n11} between planes $\{n11\}$ and $\{100\}$, etch rates and ratios of undercut and etch depth

Crystallographic plane $\{n11\}$	$\gamma_{n11} / ^\circ$		$r_{n11} / \mu\text{m min}^{-1}$ [17]	U_{n11} [20]
	Theoretical	From reference [17]		
$\{311\}$	72.5	74.2	0.93	2.10
$\{411\}$	76.4	78.7	0.85	1.89
$\{511\}$	78.9	80.9	0.81	1.78
$\{611\}$	80.7	81.0	0.73	1.61
$\{711\}$	82.0	83.1	0.69	1.52

Transition from $\{n11\}$ to $\{100\}$ is smooth, as it can be observed in Figures 3b and 5b. These transitions present facets with a weak curvature (FWC) [9] at every joint between $\{n11\}$ and $\{100\}$ planes. At a predetermined etch depth d_c (presented in Figure 2b), which is smaller than the total etches depth d_{100} , the shared $\{100\}$ plane disappears and two prismoids are separated. The etch depth d_c determines the facets with a weak curvature at the $\{100\}$ bottom of a silicon microchannel, as shown in Figure 6. The larger etch depth value d_c implies the larger size of FWC at the cross-sectional shapes of the obtained obstacles at the bottom of the microchannel. The FWC and controlled obstacles can affect fluid flow in the fabricated microchannel in different ways because of different sizes and 3D shapes. The value of d_c should be the result of a trade-off between the smallest distance between obstacles and the size of facets with a weak curvature.

Vertices of acute and obtuse angles in the masking layer are changing their position during etching ($A \rightarrow B$, $C \rightarrow D$ and $E \rightarrow F, G$ in Figure 2b). The position of vertices F and G depends on etch rates of $\{n11\}$ and $\{100\}$ crystallographic planes:

$$X_{E \rightarrow F} = X_{E \rightarrow G} = \frac{d_{n10}}{\sin \alpha_{n10}} - \frac{d_c}{\text{tg} \alpha_{n10}} + \frac{d_{100} - d_c}{\text{tg} \alpha_{n10}} = d_{100} \left(\frac{U_{n11}}{\sin \alpha_{n10}} + \frac{1 - \frac{2d_c}{d_{100}}}{\text{tg} \alpha_{n10}} \right) \quad (8)$$

$$Y_{E \rightarrow F} = Y_{E \rightarrow G} = d_c - (d_{100} - d_c) = 2d_c - d_{100} \quad (9)$$

$$d_{FG} = 2d_{100} \left(\frac{U_{n11}}{\sin \alpha_{n10}} + \frac{1 - 2\frac{d_c}{d_{100}}}{\text{tg} \alpha_{n10}} \right) = 2d_{100} \left(\frac{U_{n11}}{\sin \alpha_{n10}} + \frac{1}{\text{tg} \alpha_{n10}} \right) - \frac{4d_c}{\text{tg} \alpha_{n10}} \quad (10)$$

where $X_{E \rightarrow F}$, $X_{E \rightarrow G}$ and $Y_{E \rightarrow F,G}$ are absolute displacements of vertices in x and y directions (<100> crystallographic directions) and d_{FG} is the distance between vertices F and G at the end of etching. Reduction of the distance between fabricated prismoids, Δd , is:

$$\Delta d = d_{MQ} - d_{FG} = \frac{4d_c}{\text{tg} \alpha_{n10}} + d_{NP} \quad (11)$$

These analytical relations allow the dimension control during etching of the silicon structure in anisotropic TMAH 25 wt.% aqueous solution. Before etching, we performed level set simulations using two designed patterns in Figures 3 and 5. The presented simulations are carried out for crystallographic directions <410> and <100> in the case of the first pattern and for crystallographic directions <610> and <100> in the case of the second pattern. Pictures of the simulated etching profiles are rendered by the Paraview visualization package [44].

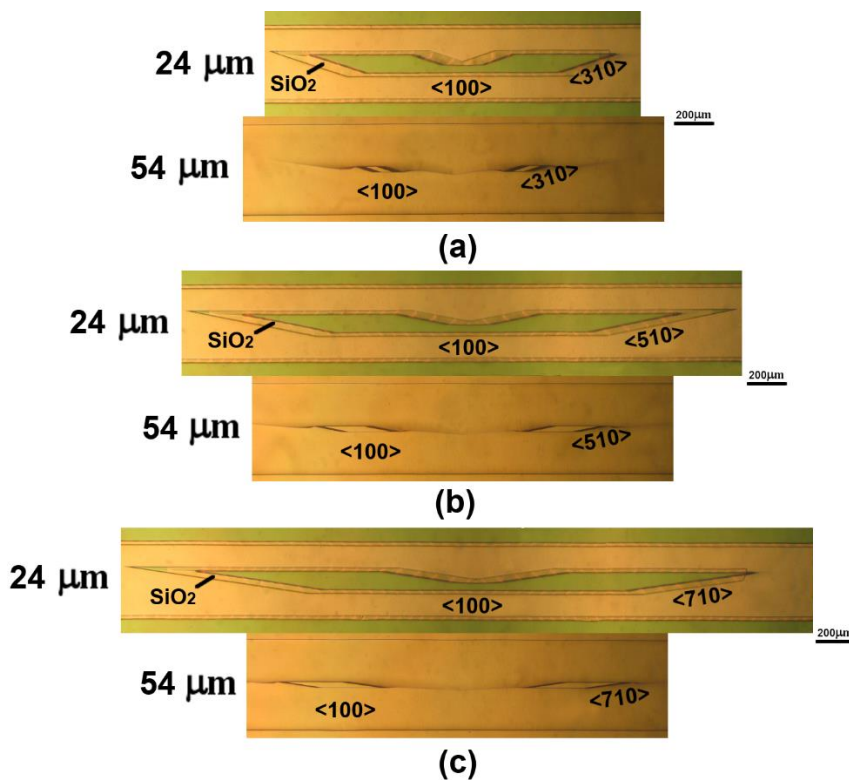


Figure 4. Microphotographs of the first basic pattern with the sides along crystallographic directions <100> and: a) <310>, b) <510>, c) <710>. The SiO₂ masking layer is present for the etch depth of 24 μm. SiO₂ is removed after reaching the etch depth of 54 μm.

In the presented example for the developed etching technique, a predetermined etch depth d_c is 40 μm in our simulations and experiments, while the total etch depth d_{100} is 54 μm. We simulated the first and the second basic pattern

designed within the square aperture with the sides along $\langle 110 \rangle$ crystallographic directions. In the experiments, we etched both basic patterns that are inside the microchannels with sides along $\langle 100 \rangle$ crystallographic directions. There is a good agreement between experiments and simulations, as shown in Figures 3 and 5. Table 2 provides distances d_{FG} that are calculated using eq. (10) and parameters shown in Table 1 and measured in experiments. Figure 5 shows the evolution of the simulated etching profile based on the basic pattern for matrix of obstacles. Also, in Figure 5, we presented two shear rows of silicon obstacles integrated in the microchannel fabricated using the second basic pattern.

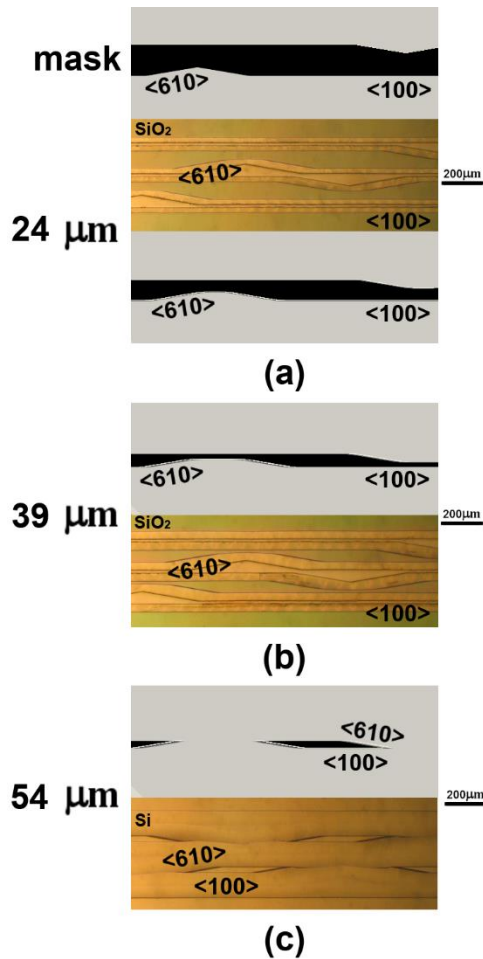


Figure 5. Simulated etching profiles and microphotographs of the second basic pattern with the sides along $\langle 100 \rangle$ and $\langle 610 \rangle$ crystallographic directions: a) Initial mask in SiO_2 masking layer and 3D silicon structure after etching of $24 \mu\text{m}$. b) The etch depth is $39 \mu\text{m}$. c) The etch depth is $54 \mu\text{m}$. SiO_2 is removed after reaching the etch depth of $54 \mu\text{m}$.

Table 2. Angles between $\langle n10 \rangle$ and $\langle 100 \rangle$, calculated and measured distances d_{FG} .

Crystallographic direction $\langle n10 \rangle$	$\alpha_{n10} / ^\circ$	$d_{FGc} / \mu\text{m}$	$d_{FGm} / \mu\text{m}$
$\langle 310 \rangle$	18.4	552	582
$\langle 410 \rangle$	14.0	643	645
$\langle 510 \rangle$	11.3	701	685
$\langle 610 \rangle$	9.5	717	723
$\langle 710 \rangle$	8.1	802	760

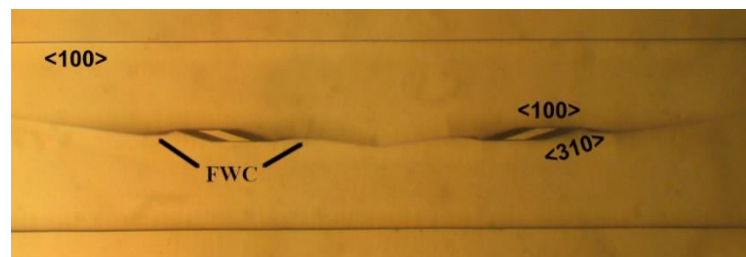


Figure 6. Ridges defined by FWC at the enlarged microphotograph of the first basic pattern with the sides along crystallographic directions $\langle 100 \rangle$ and $\langle 310 \rangle$ for the etch depth of $54 \mu\text{m}$.

The presented technique of controlled etching enables fabrication of silicon microchannels with integrated matrix of obstacles. The analysed patterns could be used for future designs of lab-on-chip platforms based on obstacles for applications such as micromixers [32–37], DLD separators [38–41] and cell peg [42]. Combination of basic patterns with sides along $\langle n10 \rangle$ and $\langle 100 \rangle$ crystallographic directions will also provide more freedom in design. Possibility to shear rows of patterns is one more potential for various arrangements of obstacles. Most of fabricated silicon platforms with obstacle like structures were performed by using dry etching [45]. Anisotropic wet etching of silicon in 25 wt.% TMAH aqueous solution is a more cost-effective process. Most of microfluidic platforms use SU-8 for moulding of obstacles, and PDMS as the structural material. Micromachining of silicon microchannels with obstacles using the presented technique, together with anodic bonding to Pyrex glass, allow production of more rigid platforms [46,47]. The process

of anodic bonding provides good sealing omitting gas permeability, which is not achieved in the most common platforms based on PDMS [48].

4. CONCLUSION

In this paper, we developed a technique for controlled obstacle etching using 25 wt.% TMAH aqueous solution at the temperature of 80 °C. Sides of basic patterns were designed along $\langle n10 \rangle$ ($2 \langle n \langle 8 \rangle$) and $\langle 100 \rangle$ crystallographic directions in the masking layer. The presented technique reduces the distance between fabricated obstacles. Combination of basic patterns enables fabrication of microchannels with an integrated matrix of obstacles in various arrangements. Analytical relations are determined to obtain dimensions of these integrated obstacles in microchannels. The basic patterns can be used to fabricate complex microfluidic platforms based on obstacles by a cost-effective process.

Acknowledgements: The authors acknowledge funding provided by the Institute of Physics and Institute of Chemistry, Technology and Metallurgy through the grant by the Ministry of Education, Science and Technological Development of the Republic of Serbia (Grant No. 451-03-68/2020-14/200026).

REFERENCES

- [1] Zubel I. Anisotropic etching of Si. *J. Micromech. Microeng.* 2019; 29: 093002.
- [2] Gosalvez MA, Zubel I, Viinikka E. Wet Etching of Silicon. In: Lindroos V, Tilli M, Lehto A, Motooka T, William A., ed. *Handbook of Silicon Based MEMS Materials and Technologies*. (William Andrew, Elsevier); 2010:375-407.
- [3] Frühauf J. *Shape and Functional Elements of the Bulk Silicon Microtechnique*. Berlin: Springer-Verlag, Berlin; 2005.
- [4] Pal P, Sato K. *Silicon wet etching for MEMS*. Pan Stanford Publishing, Singapore: Taylor&Francis; 2017.
- [5] Shikida M, Sato K, Tokoro K, Uchikawa D. Differences in anisotropic etching properties of KOH and TMAH solutions. *Sensors and Actuators A*. 2000; 80: 179-188.
- [6] Sato K, Shikida M, Yamashiro T, Asaumi K, Iriye Y, Yamamoto M. Anisotropic etching rates of single-crystal silicon for TMAH water solution as a function of crystallographic orientation. *Sensors and Actuators A*. 1999; 73: 131-137.
- [7] Resnik D, Vrtacnik D, Aljancic U, Amon S. Wet etching of silicon structures bounded by $\{311\}$ sidewalls. *Microelectronic Engineering*. 2000; 51-52: 555-566.
- [8] Resnik D, Vrtacnik D, Amon S. Morphological study of $\{311\}$ crystal planes anisotropically etched in $\{100\}$ silicon: role of etchants and etching parameters. *J. Micromech. Microeng.* 2000; 10: 430-439.
- [9] Smiljanić MM, Jović V, Lazić Ž. Maskless convex corner compensation technique on a $\{100\}$ silicon substrate in a 25 wt.% TMAH water solution. *J. Micromech. Microeng.* 2012; 22: 115011.
- [10] Smiljanić MM, Radjenović B, Radmilović-Radjenović M, Lazić Ž, Jović V. Simulation and experimental study of maskless convex corner compensation in TMAH water solution. *J. Micromech. Microeng.* 2014; 24: 115003.
- [11] Yang H, Bao M, Shen S, Li X, Zhang D, Wu G. A novel technique for measuring etch rate distribution of Si. *Sensors and Actuators A*. 2000; 79: 136-140.
- [12] Landsberger LM, Naseh S, Kahrizi M, Paranjape M. On Hillocks Generated During Anisotropic Etching of Si in TMAH. *IEEE J. Microelectromech. Syst.* 1996; 5: 106-116.
- [13] Zubel I, Barycka I, Kotowska K, Kramkowska M. Silicon anisotropic etching in alkaline solution IV: The effect of organic and inorganic agents on silicon anisotropic etching process. *Sensors and Actuators A*. 2001; 87: 163-171.
- [14] Shen J, Chen Y, Zhang F, Zhang D, Gan Y. Morphological and crystallographic evolution of patterned silicon substrate etched in TMAH solutions. *Applied Surface Science*. 2019; 496: 143720.
- [15] Trieu HK, Mokwa W. A generalized model describing corner undercutting by the experimental analysis of TMAH/IPA. *J. Micromech. Microeng.* 1998; 8: 80-83.
- [16] Sarro PM, Brida D, Vlist W vd, Brida S. Effect of surfactant on surface quality of silicon microstructures etched in saturated TMAHW solutions. *Sensors and Actuators A*. 2000; 85: 340-345.
- [17] Smiljanić MM, Radjenović B, Radmilović-Radjenović M, Lazić Ž, Jović V. Evolution of Si crystallographic planes-etching of square and circle patterns in 25 wt.% TMAH. *Micromachines* 2019; 10(2): 102.
- [18] Pal P, Sato K, Gosalvez MA, Shikida M. Study of rounded concave and sharp edge convex corners undercutting in CMOS compatible anisotropic etchants. *J. Micromech. Microeng.* 2007; 17: 2299–2307.
- [19] Smiljanić MM, Lazić Ž, Radjenović B, Radmilović-Radjenović M, Jović V, Rašljic M, Cvetanović Zobenica K, Filipović A. Etched Parallelogram Patterns with Sides Along $\langle 100 \rangle$ and $\langle n10 \rangle$ Directions in 25 wt.% TMAH. In: *Proc. 6th Conf. IcETran*, Srebrno jezero, Serbia, Jun. 3–6. 2019.
- [20] Smiljanić MM, Lazić Ž, Jović V, Radjenović B, Radmilović-Radjenović M. Etching of Uncompensated Convex Corners with Sides along $\langle n10 \rangle$ and $\langle 100 \rangle$ in 25 wt% TMAH at 80 °C. *Micromachines* 2020; 11(3): 253.

- [21] Powell O, Harrison HB. Anisotropic etching of {100} and {110} planes in (100) silicon. *J Micromech. Microeng.* 2001; 11: 217-220.
- [22] Mukhiya R, Bagolini A, Margesin B, Zen M and Kal S 2006 <100> bar corner compensation for CMOS compatible anisotropic TMAH etching. *J. Micromech. Microeng.* 16 2458-2462.
- [23] Bagolini A, Faes A, Decarli M. Influence of Etching Potential on Convex Corner Anisotropic Etching in TMAH Solution. *IEEE J. Microelectromech. Syst.* 2010; 19: 1254-1259.
- [24] Mukhiya R, Bagolini A, Bhattacharyya TK, Lorenzelli L, Zen M. Experimental study and analysis of corner compensation structures for CMOS compatible bulk micromachining using 25 wt.% TMAH. *Microelectronics Journal* 2011; 42:127-134.
- [25] Merlos A, Acero M C, Bao M H, Bausells J, Esteve J. A study of the undercutting characteristics in the TMAH-IPA system. *J. Micromech. Microeng.* 1992; 2: 181-183.
- [26] Merlos A, Acero M C, Bao MH, Bausells J, Esteve J. TMAH/IPA anisotropic etching characteristics. *Sensors and Actuators A.* 1993; 37-38: 737-743.
- [27] Pal P, Sato K, Shikida M, Gosalvez MA. Study of corner compensating structures and fabrication of various shape of MEMS structures in pure and surfactant added TMAH. *Sensors and Actuators A.* 2009; 154: 192-203.
- [28] Pal P, Sato K, Chandra S. Fabrication techniques of convex corners in a (100)-silicon wafer using bulk micromachining: a review. *J. Micromech. Microeng.* 2007; 17: R111-R133.
- [29] Osher S, Sethian JA, Fronts Propagating with Curvature Dependent Speed: Algorithms Based on Hamilton-Jacobi Formulations. *J. Comp. Phys.* 1988; 79: 12-49.
- [30] Radjenović B, Radmilović-Radjenović M, Mitrić M. Non-convex Hamiltonians in 3D level set simulations of the wet etching of silicon. *Appl. Phys. Lett.* 2006; 89: 213102.
- [31] Radjenović B, Radmilović-Radjenović M, Mitrić M. Level set approach to anisotropic wet etching of silicon. *Sensors* 2010; 10 (5): 4950-4967.
- [32] Bernacka-Wojcik I, Ribiero S, Wojcik PJ, Alves PU, Busani T, Fortunato E, Viana Baptista P, Covas JA, Águas H, Hilliou L, Martins R. Experimental optimization of a passive planar rhombic micromixer with obstacles for effective mixing in a short channel length. *RSC Advances.* 2014; 4: 56013-56025.
- [33] Alves PU, Vinhas R, Fernandes AR, Birol SZ, Trabzon L, Bernacka-Wojcik I, Igreja R, Lopes P, Viana Baptista P, Águas, H, Fortunato E, Martins R. Multifunctional microfluidic chip for optical nanoprobe based RNA detection – application to Chronic Myeloid Leukemia. *Scientific Reports.* 2018; 8:381.
- [34] Bhagat AAS, Peterson ETK, Papautsky I. A passive planar micromixer with obstructions for mixing at low Reynolds numbers. *J. Micromech. Microeng.* 2007; 17: 1017-1024.
- [35] Wang H, Iovenitti P, Harvey E, Masood S. Optimizing layout of obstacles for enhanced mixing in microchannels. *Smart Mater. Struct.* 2002; 11:662-667.
- [36] Wang CT, Hu YC. Mixing of liquids using obstacles in Y-type microchannels. *Tamkang Journal of Science and Engineering.* 2010; 13: 385-394.
- [37] Jeon W, Burm Shin C. Design and simulation of passive mixing in microfluidic systems with geometric variation. *Chemical Engineering Journal.* 2009; 152: 575-582.
- [38] McGrath J, Jimenez M, Bridle H. Deterministic lateral displacement for particle separation: a review. *Lab on a chip.* 2014; 4: 4139.
- [39] Zhang Z, Chien W, Henry E, Fedosov DA, Gompper G. Sharp-edged geometric obstacles in microfluidics promote deformability-based sorting of cells. *Physical Review Fluids.* 2019; 4: 024201.
- [40] Guo Q, Duffy SP, Matthews K, Islamzada E, Ma H. Deformability based cell sorting using microfluidic ratchets enabling phenotypic separation of leukocytes directly from whole blood. *Scientific Reports.* 2017; 7: 6627.
- [41] Jiang J, Zhao H, Shu W, Tian J, Huang Y, Song Y, Wang R, Li E, Slamon D, Hou D, Du X, Zhang L, Chen Y, Wang Q. An integrated microfluidic device for rapid and high-sensitivity analysis of circulating tumor cells. *Scientific Reports.* 2017; 7: 42612.
- [42] Lykov K, Nematbakhsh Y, Shang M, Lim CT, Pivkin IV. Probing eukaryotic cell mechanics via mesoscopic simulations. *PLoS Comput Biol.* 2017; 3(9).
- [43] Jović V, Popović M, Lamovec J. Preciznost anizotropnog hemijskog nagrizanja.; In: *Proc. 52nd Conf. ETRAN*, Palić, Serbia, June 8-12, 2008, MO2.6-1-4. (in Serbian)
- [44] Open source, multi-platform data analysis and visualization application software <http://www.paraview.org>
- [45] Mihailović M, Rops CM, Hao J, Mele L, Creemer JF, Sarro PM. MEMS silicon-based micro-evaporator. *J. Micromech. Microeng.* 2011; 21: 075007.
- [46] Roh C, Lee J, Kang CK. Physical Properties of PDMS (Polydimethylsiloxane) Microfluidic Devices on Fluid Behaviors: Various Diameters and Shapes of Periodically-Embedded Microstructures. *Materials* 2016; 9: 836.
- [47] Kang CK, Roh C, Overfelt R A. Pressure-driven deformation with soft polydimethylsiloxane (PDMS) by a regular syringe pump: challenge to the classical fluid dynamics by comparison of experimental and theoretical results. *RSC Advances* 2013; 4: 3102-3112.
- [48] Merkel T C, Bondar V I, Nagai K, Freeman B D, Pinnau I Gas sorption, diffusion, and permeation in poly(dimethylsiloxane) *Polymer Physics* 2000; 38: 415-434

SAŽETAK**Kontrolisan raspored integrisanih prepreka u silicijumskim mikrokanalima nagrizanim u 25 mas.% rastvoru tetrametilamonijum hidroksida**

Milče M. Smiljanić¹, Branislav Rađenović², Žarko Lazić¹, Marija Radmilović-Rađenović², Milena Rašljic Rafajilović¹, Katarina Cvetanović-Zobenica¹, Evgenija Milinković¹ i Ana Filipović¹

¹*Institut za hemiju, tehnologiju i metalurgiju, Institut od nacionalnog značaja za Republiku Srbiju, Univerzitet u Beogradu, Njegoševa 12, 11000 Beograd, Srbija*

²*Institut za fiziku, Univerzitet u Beogradu, Pregrevica 118, 11080 Beograd, Srbija*

(Naučni rad)

U ovom radu je prezentovana i analizirana izrada silicijumskih mikrokanala sa integrisanim preprekama u vodenom rastvoru 25 mas.% tetrametilamonijum hidroksida (TMAH) na temperaturi od 80 °C. Proučavani su osnovni oblici maski koji predstavljaju uniju dva simetrična ostrva u obliku paralelograma čije su stranice duž unapred određenih kristalografskih pravaca ($2 < n < 8$) i $< 100 >$. Oštri uglovi paralelograma su manji od 45°. Izvedene su formule za izračunavanje dimenzija integrisanih prepreka. Razvijena je tehnika nagrizanja koja smanjuje rastojanje između prepreka. Pre eksperimenata izvršene su simulacije osnovnih oblika koje se baziraju na metodi implicitno definisanih nivoa (engl. level set method). Prezentovan je razvoj nagrizanih osnovnih oblika maski za unapred određene kristalografske pravce $< n10 >$. Kombinacija osnovnih oblika maski čije su stranice duž kristalografskih pravaca $< 610 >$ i $< 100 >$ je iskorišćena za izradu dva reda matrice silicijumskih prepreka u mikrokanalu. Dobijeno je dobro slaganje između eksperimenata i simulacija. Dobijeni rezultati omogućavaju jednostavnu i jeftinu izradu različitih kompleksnih mikrofluidnih silicijumskih platformi sa integrisanim preprekama.

Ključne reči: vlažno hemijsko nagrizanje; simulacija na bazi implicitno definisanih nivoa; 3D silicijumske strukture; mikrofluidna platforma